

Production of the doubly charged Δ baryon in e^+e^- annihilation at energies from 2.3094 to 2.6464 GeV

M. Ablikim *et al.**
(BESIII Collaboration)

 (Received 23 May 2023; accepted 15 September 2023; published 11 October 2023)

The processes $e^+e^- \rightarrow \Delta^{++}\bar{\Delta}^{--}$ and $e^+e^- \rightarrow \Delta^{++}\bar{p}\pi^- + \text{c.c.}$ are studied for the first time with 179 pb^{-1} of e^+e^- annihilation data collected with the BESIII detector at center-of-mass energies from 2.3094 to 2.6464 GeV. No significant signal for the $e^+e^- \rightarrow \Delta^{++}\bar{\Delta}^{--}$ process is observed and the upper limit of the Born cross section is estimated at each energy point. For the process $e^+e^- \rightarrow \Delta^{++}\bar{p}\pi^- + \text{c.c.}$, a significant signal is observed at center-of-mass energies near 2.6454 GeV and the corresponding Born cross section is reported.

DOI: 10.1103/PhysRevD.108.072010

I. INTRODUCTION

Baryons, specifically the proton and neutron, are the basic building blocks of matter. These half-integer spin fermions are comprised of three valence quarks bound together by the strong interaction. The most common baryons are the ones from the spin 1/2 SU(3) octet, whose properties have been extensively studied in electron-positron collision experiments [1]. The cross section line shape of many baryon pair production processes seem to display the common feature of a plateau starting from threshold, including $p\bar{p}$ [2], $n\bar{n}$ [3], $\Lambda\bar{\Lambda}$ [4], $\Sigma\bar{\Sigma}$ [5], $\Xi\bar{\Xi}$ [6], and $\Lambda_c^+\bar{\Lambda}_c^-$ [7].

However, the baryon decuplet, which is comprised of the spin 3/2 SU(3) baryons, is not fully investigated in electron-positron collisions. Compared to the baryon octet, the decuplet is a simpler system as the wave functions of the decuplet baryons are symmetric under flavor exchange. The lightest member of the decuplet is the Δ baryon with a mass of $1232 \text{ MeV}/c^2$, which is heavier than the nucleon by about $300 \text{ MeV}/c^2$. Experimental information on Δ baryons comes mostly from experiments in the spacelike region [8], but rarely from the timelike region. The e^+e^- annihilation process can provide information on timelike form factors of the Δ , similar to the practice for octet baryons [1].

In a naive perturbative description of the e^+e^- annihilation into baryons, the virtual timelike photon is first

coupled to a primary $q\bar{q}$ pair, which then hadronizes by popping two additional quark-antiquark pairs from the vacuum. The total perturbative cross section σ at a given c.m. energy \sqrt{s} is obtained by superposing the amplitudes with different flavors q in the primary $q\bar{q}$ pair and squaring the result, $\sigma(e^+e^- \rightarrow N\bar{N}) \propto |\sum Q_q a_q^N(s)|^2$, where a_q^N represents the amplitude of producing the baryon N with a given primary flavor q and Q_q denotes the charge of flavor q . These amplitudes are determined by the baryon wave functions [9]. Since Δ baryons have totally symmetric wave functions, the corresponding amplitudes are equal, $a_u^\Delta = a_d^\Delta \equiv a^\Delta$. For all four members of the Δ multiplet, $\Delta^{++}, \Delta^+, \Delta^0, \Delta^-$, their relative yields predicted by perturbative theory are $\Delta^{++}:\Delta^+:\Delta^0:\Delta^- = 4:1:0:1$ [9,10]. However, the relative yield within the multiplet can also be obtained by the relevant Clebsch-Gordan coefficients [11] and corrected by the corresponding reduced matrix elements for isospin 1 and 0. For Δ baryons, one expects the relative yields $\sigma(\Delta^{++}) = \sigma(\Delta^-)$ and $\sigma(\Delta^+) = \sigma(\Delta^0)$ from the Clebsch-Gordan decomposition even without the precise values of the reduced matrix elements [9]. This contradicts the perturbative prediction.

A more detailed discussion of baryon pair production is carried out by Körner and Kuroda in Ref. [12], including the baryon decuplet. Since the Δ states are spin 3/2 baryons, four form factors are required to fully describe their structure. In the framework of the generalized vector-dominance model, the form factors can be predicted by assuming they arise from the coupling of many vector mesons in the form of a product of poles. Within the generalized vector-dominance model, the $e^+e^- \rightarrow \Delta^{++}\bar{\Delta}^{--}$ process has the largest cross section in the baryon decuplet due to the relatively light mass and double charge of the Δ^{++} baryon, which can reach tens of pb near the threshold.

*Full author list given at the end of the article.

Published by the American Physical Society under the terms of the Creative Commons Attribution 4.0 International license. Further distribution of this work must maintain attribution to the author(s) and the published article's title, journal citation, and DOI. Funded by SCOAP³.

TABLE I. Dataset and expected cross section. The symbol \sqrt{s} is the c.m. energy. \mathcal{L} is the integrated luminosity. σ^{theory} is the cross section of the $e^+e^- \rightarrow \Delta^{++}\bar{\Delta}^{--}$ process predicted in Ref. [12].

\sqrt{s} (GeV)	\mathcal{L} (pb $^{-1}$)	σ^{theory} (pb)
2.3094	21.1	0.0
2.3864	22.5	0.0
2.3960	66.9	0.0
2.5000	1.10	19.7
2.6444	33.6	5.7
2.6464	34.1	5.6

The energy threshold of Δ^{++} pair production is accessible at BESIII and datasets at different energies have been collected to study baryon pair production. The predicted cross section for $e^+e^- \rightarrow \Delta^{++}\bar{\Delta}^{--}$ may be accessible at BESIII, providing a first step toward extraction of the production ratios within the Δ multiplet in order to test theoretical predictions. In this paper, we present a search for the process $e^+e^- \rightarrow \Delta^{++}\bar{\Delta}^{--}$ with the subsequent decay $\Delta^{++} \rightarrow p\pi^+$ based on data samples collected with the BESIII detector at 6 c.m. energies from 2.3094 to 2.6464 GeV, corresponding to a total integrated luminosity of 179 pb $^{-1}$ [13,14], as listed in Table I. Simultaneously, the single Δ processes, $e^+e^- \rightarrow \Delta^{++}\bar{p}\pi^-$ and its charge conjugate (c.c.), are also studied.

II. DETECTOR AND DATA SAMPLES

The BESIII detector [15] records symmetric e^+e^- collisions provided by the BEPCII storage ring [16], which operates in the c.m. energy range from 2.0 to 4.95 GeV, with a peak luminosity of 1×10^{33} cm $^{-2}$ s $^{-1}$ achieved at $\sqrt{s} = 3.77$ GeV. BESIII has collected large data samples in this energy region [17]. The cylindrical core of the BESIII detector covers 93% of the full solid angle and consists of a helium-based multilayer drift chamber (MDC), a plastic scintillator time-of-flight system (TOF), and a CsI(Tl) electromagnetic calorimeter, which are all enclosed in a superconducting solenoidal magnet providing a 1.0 T magnetic field [18]. The solenoid is supported by an octagonal flux-return yoke with resistive plate counter muon identification modules interleaved with steel. The charged-particle momentum resolution at 1 GeV/c is 0.5%, and the specific ionization energy (dE/dx) resolution is 6% for electrons from Bhabha scattering. The electromagnetic calorimeter measures photon energies with a resolution of 2.5% (5%) at 1 GeV in the barrel (end cap) region. The time resolution in the TOF barrel region is 68 ps, while that in the end cap region is 110 ps.

The GEANT4-based [19] simulation software package BOOST [20], which includes the geometric and material description of the BESIII detector and the detector response, is used to produce Monte Carlo (MC) simulated

data samples. The initial particles are provided by process-dependent generators, then treated with BOOST. Exclusive MC samples are generated using the ConExc generator [21] with initial state radiation and vacuum polarization taken into account to determine the detection efficiencies and to provide shapes of the involved processes. Inclusive hadron production of the type $e^+e^- \rightarrow$ hadrons is simulated by a hybrid generator [22] to estimate possible background processes and to optimize event selection criteria. The beam energy spread of BEPCII is less than 1 MeV at $\sqrt{s} < 3$ GeV, which is much smaller than the experimental resolution of the BESIII detector and can be ignored in the simulation.

III. EVENT SELECTION

For the $e^+e^- \rightarrow \Delta^{++}\bar{\Delta}^{--}$ process (with the subsequent decay $\Delta^{++} \rightarrow p\pi^+ + \text{c.c.}$), the final state $p\bar{p}\pi^+\pi^-$ is reconstructed for the study of Δ production. Candidate events are required to have exactly four reconstructed charged tracks detected in the acceptance of the MDC within a polar angle (θ) range of $|\cos\theta| < 0.93$, where θ is defined with respect to the z axis, which is the symmetry axis of the MDC. For these tracks, the distance of closest approach to the interaction point must be less than 10 cm along the z axis, and less than 1 cm in the transverse plane. Particle identification (PID) combines measurements of the dE/dx in the MDC and the flight time in the TOF to calculate a likelihood $\mathcal{L}(h)$ ($h = p, K, \pi$) for each hypothesis of a hadron h . Tracks are identified as protons when the proton hypothesis has the greatest likelihood [$\mathcal{L}(p) > \mathcal{L}(K)$ and $\mathcal{L}(p) > \mathcal{L}(\pi)$]. Charged pions are identified by comparing the pion and kaon hypothesis likelihoods of the remaining tracks, requiring $\mathcal{L}(\pi) > \mathcal{L}(K)$. Exactly two oppositely charged pions and one proton-antiproton pair are required in each event. To improve the momentum and energy resolution and to suppress background events, a four-constraint (4C) kinematic fit imposing four-momentum conservation is performed under the hypothesis $e^+e^- \rightarrow p\bar{p}\pi^+\pi^-$. The χ^2 of the kinematic fit is required to be less than 50. The semi- Δ process, i.e. $e^+e^- \rightarrow \Delta^{++}\bar{p}\pi^-$ and its charge conjugate, can be studied simultaneously since it has the same final state particles and similar kinematics.

The characteristic signal is expected to appear in the invariant mass spectrum of the $p\pi$ combination, which is denoted as $m(p\pi)$. The two-dimensional (2D) distributions of $m(p\pi^+)$ vs $m(\bar{p}\pi^-)$ and $m(p\pi^-)$ vs $m(\bar{p}\pi^+)$ of the events selected from data at $\sqrt{s} = 2.6444$ GeV are shown in Fig. 1 as an example. An enhancement around the nominal Δ baryon mass is visible in the doubly charged combination of $p\pi$ (left plot) while the Λ signal is visible in the neutral combination (right plot). Potential background reactions to the $e^+e^- \rightarrow \Delta^{++}\bar{\Delta}^{--}$ process are studied using inclusive $e^+e^- \rightarrow$ hadrons MC samples. Simulated events are subject to the same selection procedure as that applied

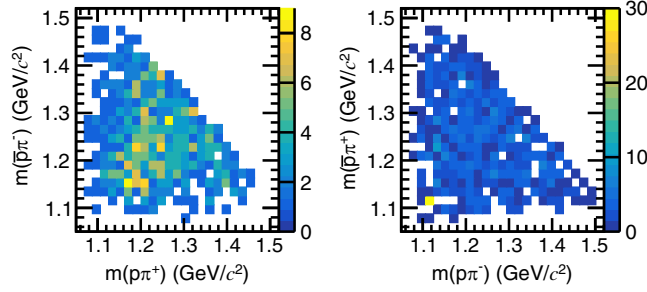


FIG. 1. Two-dimensional distributions of $m(\bar{p}\pi^-)$ vs $m(p\pi^+)$ (left) and $m(\bar{p}\pi^+)$ vs $m(p\pi^-)$ (right) for the candidate events selected from data taken at $\sqrt{s} = 2.6444$ GeV.

to the experimental data. According to MC simulations, the dominant background stems from $e^+e^- \rightarrow \Delta^{++}\bar{p}\pi^- + c.c.$, $\Lambda\bar{\Lambda}$, and $p\bar{p}\pi^+\pi^-$ processes, which have the same final state particles as the signal reaction. Other background channels like $e^+e^- \rightarrow \rho^0 p\bar{p}$, $\Delta^0 \bar{p}\pi^+ + c.c.$, and $\Delta^0 \bar{\Delta}^0$ are also possible but rare, according to the inclusive hybrid MC sample described earlier.

IV. SIGNAL YIELD AND CROSS SECTION

Since the data samples in both 2D distributions are identical, there is a correlation between them, which can potentially impact the statistical uncertainty in signal extraction. The extent of this influence is contingent upon the correlation of the shapes exhibited by different variable distributions. In the case of the $p\bar{p}\pi^+\pi^-$ final state, the variation in spectrum shapes among the different components is not significant in spectra other than the invariant mass spectrum that contains the resonant peak due to the final state being a 4-body system with numerous degrees of freedom. Consequently, the presence of the correlation does not significantly affect the statistical uncertainty. Nonetheless, the correlation can help to constrain the yields of the components in a 2D simultaneous fit. To determine the signal yield of the $e^+e^- \rightarrow \Delta^{++}\bar{\Delta}^{--}$ process, a simultaneous unbinned maximum likelihood fit is performed to the 2D distributions of $m(\bar{p}\pi^-)$ vs $m(p\pi^+)$ and $m(\bar{p}\pi^+)$ vs $m(p\pi^-)$. This procedure is repeated at each energy point. In the fit, the yields of corresponding components in both 2D spectra are obtained with shared parameters. The signal is modeled with the MC-derived shape of $m(\bar{p}\pi^-)$ vs $m(p\pi^+)$ and $m(\bar{p}\pi^+)$ vs $m(p\pi^-)$ for the $e^+e^- \rightarrow \Delta^{++}\bar{\Delta}^{--}$ process. The background is described by the MC-simulated shape of four dominant components, which are phase space (PHSP) ($e^+e^- \rightarrow p\bar{p}\pi^+\pi^-$), semi- Δ ($e^+e^- \rightarrow \Delta^{++}\bar{p}\pi^-$ and $p\pi^+\bar{\Delta}^{--}$, also with the phase space model), and $e^+e^- \rightarrow \Lambda\bar{\Lambda}$, while other rarer components are neglected since their distributions are similar to those of the phase space. In the analysis, the interference among different components is neglected, considering the spin of the combination of a proton and a pion ($p\pi$) tends to be

$1/2$ when produced at low energy, whereas it is $3/2$ in the case of Δ decay. As a result, different components tend to be incoherently produced. Figure 2 shows the projections of $m(p\pi^+)$, $m(\bar{p}\pi^-)$, $m(p\pi^-)$, and $m(\bar{p}\pi^+)$ for the simultaneous fit to data taken at 2.6444 GeV; these indicate that the data is well described by these five components. In extraction of the $\Delta^{++}\bar{\Delta}^{--}$ signal, the yields of the semi- Δ processes, i.e. $e^+e^- \rightarrow \Delta^{++}\bar{p}\pi^- + c.c.$, is obtained simultaneously. Although the events are duplicatedly used in the two 2D distributions, the statistical uncertainties of the yields of Δ^{++} involved processes in the simultaneous fit remain unaffected. This is because the target signal, Δ^{++} , is a broad resonance resulting in a negligible discrepancy between the signal and the PHSP in the invariant mass spectra other than the characteristic one, as illustrated in Fig. 2. The yields are listed in Tables II and III. Due to the closeness of the energies, the data samples at 2.6444 and 2.6464 GeV are combined.

The statistical significance of the signal is determined by comparing the change of the negative log-likelihood value in the fit without the signal contribution and considering the change of the number of degrees of freedom. The statistical significances are listed in Tables II and III. The $\Delta^{++}\bar{\Delta}^{--}$ signal is not significant for any of the c.m. energies. A significant semi- Δ component is observed only above 2.6 GeV.

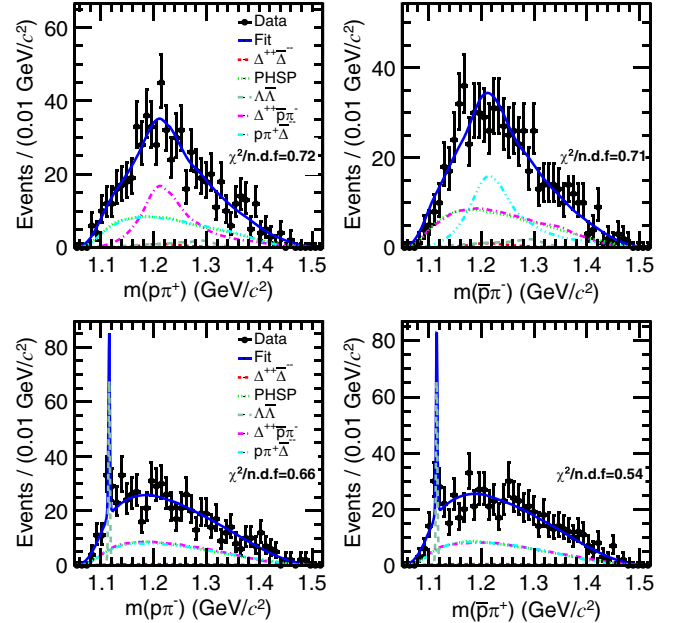


FIG. 2. Projections of the simultaneous fit to the 2D distributions of $m(\bar{p}\pi^-)$ vs $m(p\pi^+)$ and $m(\bar{p}\pi^+)$ vs $m(p\pi^-)$ of the candidate events selected from data taken at $\sqrt{s} = 2.6444$ GeV. The black dots with error bars are data. The blue solid curve is the total fit result. The dashed and dotted curves show the components as indicated in the legends, and $\chi^2/n.d.f.$ is the ratio of the χ^2 value to the number of degrees of freedom in the fit.

TABLE II. Born cross sections of $e^+e^- \rightarrow \Delta^{++}\bar{\Delta}^{--}$ at various c.m. energy points. All symbols are defined the same as those in Eq. (1). The N_{up} and σ_{up}^B are set at the 90% CL for the c.m. energy points with statistical significance less than 2σ . The branching fraction of $\Delta^{++}\bar{\Delta}^{--}$ decaying to the final state $p\bar{p}\pi^+\pi^-$ is 100.0%. The first uncertainty is statistical and the second one is systematic. The line with an asterisk is a combined result of two nearby energy points $\sqrt{s} = 2.6444$ and 2.6464 GeV.

\sqrt{s} (GeV)	N (N_{up})	ϵ	$(1 + \delta)$	σ^B (σ_{up}^B) (pb)	Significance (σ)
2.3094	$0.0_{-0.0}^{+0.3}$ (1.4)	0.009	0.869	$0.0_{-0.0}^{+1.9} \pm 0.0$ (8.7)	0.01
2.3864	$4.3_{-4.3}^{+7.9}$ (16.3)	0.059	0.864	$3.7_{-3.7}^{+6.8} \pm 0.3$ (14.1)	0.56
2.3960	$17.0_{-14.1}^{+12.8}$ (35.0)	0.068	0.865	$4.3_{-3.6}^{+3.3} \pm 0.4$ (8.9)	1.19
2.5000	$0.0_{-0.0}^{+2.3}$ (4.7)	0.172	0.919	$0.0_{-0.0}^{+13.2} \pm 0.0$ (27.1)	0.00
2.6444	$12.3_{-12.3}^{+53.3}$ (95.4)	0.280	0.962	$1.4_{-1.4}^{+5.9} \pm 0.1$ (10.5)	0.24
2.6464	$0.0_{-0.0}^{+11.4}$ (46.4)	0.282	0.962	$0.0_{-0.0}^{+1.2} \pm 0.0$ (5.0)	0.00
*2.6454	$0.0_{-0.0}^{+26.5}$ (87.3)	0.281	0.962	$0.0_{-0.0}^{+1.4} \pm 0.0$ (4.8)	0.00

TABLE III. Born cross sections of $e^+e^- \rightarrow \Delta^{++}\bar{p}\pi^- + \text{c.c.}$ at various c.m. energy points. All symbols are the same as Table II.

\sqrt{s} (GeV)	N (N_{up})	ϵ	$(1 + \delta)$	σ^B (σ_{up}^B) (pb)	Significance (σ)
2.3094	$0.0_{-0.0}^{+0.4}$ (1.8)	0.004	0.873	$0.0_{-0.0}^{+6.2} \pm 0.0$ (28.1)	0.00
2.3864	$5.2_{-5.2}^{+6.9}$ (17.0)	0.046	0.928	$5.4_{-5.4}^{+7.2} \pm 0.5$ (17.6)	0.88
2.3960	$0.0_{-0.0}^{+14.1}$ (30.7)	0.056	0.932	$0.0_{-0.0}^{+4.0} \pm 0.0$ (8.8)	0.01
2.5000	$0.0_{-0.0}^{+5.0}$ (6.5)	0.156	0.961	$0.0_{-0.0}^{+30.3} \pm 0.0$ (39.4)	0.00
2.6444	$424.8_{-109.2}^{+77.6}$	0.247	0.982	$52.1_{-13.4}^{+9.5} \pm 4.2$	3.87
2.6464	$536.0_{-58.9}^{+57.7}$	0.252	0.982	$63.6_{-7.0}^{+6.8} \pm 8.0$	6.26
*2.6454	$965.1_{-82.5}^{+81.9}$	0.249	0.982	$58.2_{-5.0}^{+4.9} \pm 5.9$	7.09

The upper limit on the signal yield of the $e^+e^- \rightarrow \Delta^{++}\bar{\Delta}^{--}$ process is determined with a Bayesian approach [23] via a likelihood scan. The systematic uncertainty is considered by choosing the most conservative result among the fit variations used to evaluate the additive uncertainties and smearing the obtained likelihood curve with a Gaussian function with the width of the multiplicative systematic uncertainty [24]. The upper limit on the signal yield at the 90% confidence level (CL), N_{up} , is determined by integrating the smeared likelihood function $L(N)$, as illustrated shown in Fig. 3. The upper limit, N_{up} , corresponds to 90% of the full integral, i.e. $\int_0^{N_{\text{up}}} L(x)dx / \int_0^\infty L(x)dx = 0.90$. The same method is applied to the $e^+e^- \rightarrow \Delta^{++}\bar{p}\pi^- + \text{c.c.}$ process at the energy points with a statistical significance less than 2σ .

The Born cross section is calculated as

$$\sigma^B = \frac{N}{\mathcal{L} \cdot \epsilon \cdot (1 + \delta) \cdot \text{Br}}, \quad (1)$$

where N is the number of signal events in data, \mathcal{L} is the integrated luminosity, ϵ is the detection efficiency, $(1 + \delta)$ is the radiative correction factor due to initial state radiation and vacuum polarization, and Br is the branching fraction

of the decay $\Delta^{++} \rightarrow p\pi^+$ (100%) [11]. Both ϵ and $1 + \delta$ are obtained from MC simulation of the signal reaction at each c.m. energy. The input Born cross section line shape for the $e^+e^- \rightarrow \Delta^{++}\bar{\Delta}^{--}$ process is a flat distribution that

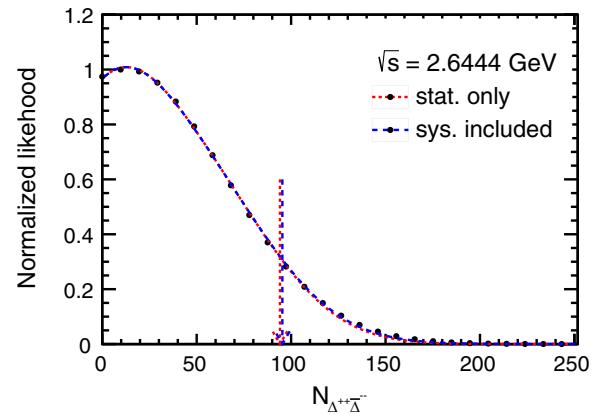


FIG. 3. Likelihood distributions vs the signal yields of the $e^+e^- \rightarrow \Delta^{++}\bar{\Delta}^{--}$ process for data taken at $\sqrt{s} = 2.6444$ GeV. The red dotted arrow indicates the upper limit at the 90% CL by only considering the statistical uncertainty, while the blue dashed arrow has incorporated the systematic uncertainty.

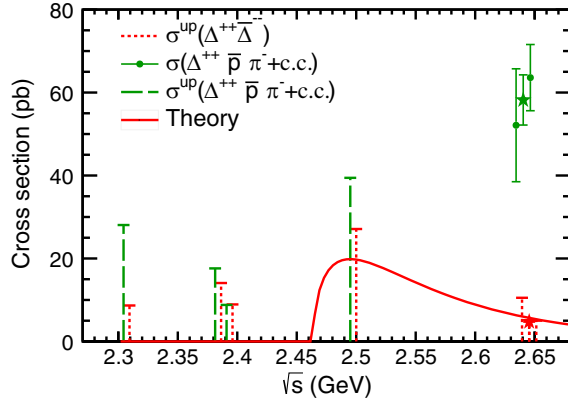


FIG. 4. Born cross sections of $e^+e^- \rightarrow \Delta^{++}\bar{\Delta}^{--}$ and $\Delta^{++}\bar{p}\pi^- + \text{c.c.}$. The green dots with solid lines represent the Born cross sections with uncertainties. The red short-dashed and green long-dashed lines show the upper limits. The red solid curve shows theoretical prediction for the $e^+e^- \rightarrow \Delta^{++}\bar{\Delta}^{--}$ process in Ref. [12]. To avoid the overlap between different processes, the c.m. energies of the $e^+e^- \rightarrow \Delta^{++}\bar{p}\pi^- + \text{c.c.}$ process are shifted left by 5 MeV. Pentagrams show combined results of two nearby energy points 2.6444 and 2.6464 GeV, and the results at the two energy points are shifted to left and right by 5 MeV, respectively.

remains constant above the threshold, which is determined by the sum of the masses of internal particles and is equal to 2.464 GeV. Below the threshold, the line shape follows a Breit-Wigner distribution centered at the threshold with a width of 0.165 GeV, representing the width of the Δ baryon pair. The line shape for the $e^+e^- \rightarrow \Delta^{++}\bar{p}\pi^- + \text{c.c.}$ process is similar but with the threshold at 2.310 GeV and the width of the Breit-Wigner distribution at 0.117 GeV. The results of Born cross sections and upper limits for $e^+e^- \rightarrow \Delta^{++}\bar{\Delta}^{--}$ and $e^+e^- \rightarrow \Delta^{++}\bar{p}\pi^- + \text{c.c.}$ are reported in Tables II and III, respectively, and are also shown in Fig. 4.

V. SYSTEMATIC UNCERTAINTY

Various sources of systematic uncertainties concerning the measurement of the Born cross sections are investigated, including event selection criteria, integrated luminosity, radiative correction factor, branching fraction, fit procedure, and the mass and width of the Δ^{++} baryon.

The uncertainty due to differences between data and MC simulation for the tracking efficiency and PID are investigated using the high-purity control samples of $e^+e^- \rightarrow K^+K^-\pi^+\pi^-$ [13,25] for pions and $e^+e^- \rightarrow p\bar{p}\pi^+\pi^-$ [26] for protons, which are assigned as 1.0% and 1.0%, per track, respectively. The uncertainty associated with the χ^2 requirement on 4C kinematic fit is also studied by comparing the difference between data and MC simulation. A Gaussian function is convolved with the MC-simulated χ^2 shape to better match the data for the χ^2 distribution. The change of efficiency with the Gaussian-smearred MC shape is taken as the uncertainty, and ranges from 0.5% to 2.3%.

The integrated luminosity of data at each energy point is measured using large-angle Bhabha events with an uncertainty of 0.8% following the method in Ref. [14].

The uncertainty of the radiative correction factor is obtained by altering the Born cross section line shape in the MC simulation. In the $\Delta^{++}\bar{\Delta}^{--}$ case, the nominal line shape is flat above the threshold with a Breit-Wigner tail below, considering the broad width of the Δ baryon. Although Ref. [12] predicted a line shape for the baryon pair production, the shape does not consider the width of the Δ baryon and becomes 0 below threshold. To estimate the uncertainty, the shape is replaced by a more general power-law shape for a baryon pair production [27], which is motivated by perturbative quantum chromodynamics and represents the power-law asymptotic behaviour of baryons, convolved with the Breit-Wigner resonance shape of the Δ baryon. In the semi- Δ case, a three-body PHSP distribution is chosen as an alternative line shape to replace the nominal flat distribution. The three-body PHSP distribution is an integral of two cascaded quasi-two-body PHSP distributions, i.e. $\sigma \propto \int PS(\sqrt{s}, m_{p\pi}, m_\Delta) \cdot PS(m_{p\pi}, m_p, m_\pi) dm_{p\pi}^2$ with $PS(m_a, m_b, m_c)$ to be the two-body PHSP factor of the $a \rightarrow b + c$ process [28]. The difference of the product of the efficiency and radiative correction factor after changing the line shapes is taken as the uncertainty, which is around 1% at most energy points.

The uncertainty associated with the branching fraction of $\Delta^{++} \rightarrow p\pi^+$ is negligible since this is the only allowed decay mode. The uncertainty from the unknown polar angle, θ_Δ , distribution of the Δ baryon is estimated by dividing the difference of efficiencies between the two extreme angular distributions, $(1 + \cos^2\theta_\Delta)$ and $(1 - \cos^2\theta_\Delta)$, by $\sqrt{12}$ assuming a uniform probability distribution [29], giving uncertainties in the range of 3.8–10.7%.

Uncertainties due to the choice of the signal and background shapes are estimated by smearing the shapes with a Gaussian function determined from the difference of the Δ peak in data and MC simulation. The difference on the yields of the $e^+e^- \rightarrow \Delta^{++}\bar{p}\pi^- + \text{c.c.}$ process in the signal extraction is taken as the uncertainty, and is less than 1% above 2.6 GeV. Since there is almost no signal below 2.6 GeV, the relative systematic uncertainty is not estimated. The uncertainty of the $e^+e^- \rightarrow \Delta^{++}\bar{\Delta}^{--}$ process is quoted from that of the $e^+e^- \rightarrow \Delta^{++}\bar{p}\pi^- + \text{c.c.}$ process.

Since the Δ is a wide resonance, the uncertainty due to its mass and width is estimated by using the values in Ref. [30] in simulation. Specifically, the mass and width are changed from 1.2310 GeV/ c^2 and 0.1150 GeV, respectively, to 1.2308 GeV/ c^2 and 0.1109 GeV. Then the uncertainty is estimated with the same method for the shapes, and is in the range of 1.5–4.7% above 2.6 GeV and ignored at lower energies. The influence of intermediate states is checked for small contributions shown in inclusive hadronic MC samples and several possible resonances. Among the small contributions, the $\rho^0 p\bar{p}$ component has relatively large

TABLE IV. Relative systematic uncertainties, in %, for the Born cross section measurements. Column Trk is the uncertainty from tracking, PID from particle identification, 4C from the 4C kinematic fit, \mathcal{L} from luminosity, $(1 + \delta)$ from radiation correction factor, α from angular distribution of baryons, Shape from signal and background shapes in the fit, MW from the mass and width of Δ^{++} used in simulation, and R from possible intermediate states. For $(1 + \delta)$, MW, R and Total, the two numbers before and after “/” are for the processes of $e^+e^- \rightarrow \Delta^{++}\bar{\Delta}^{--}$ and $\Delta^{++}\bar{p}\pi^- + c.c.$, respectively.

\sqrt{s} (GeV)	Trk	PID	4C	\mathcal{L}	$(1 + \delta)$	α	Shape	MW	R	Total
2.3094	4.0	4.0	1.7	0.8	0.5/7.6	10.7/...	12.3/14.5
2.3864	4.0	4.0	1.4	0.8	1.4/1.2	6.2/...	8.7/8.7
2.3960	4.0	4.0	1.5	0.8	1.1/1.2	6.3/...	8.7/8.7
2.5000	4.0	4.0	2.3	0.8	0.8/0.6	3.8/...	7.3/7.3
2.6444	4.0	4.0	0.5	0.8	0.1/0.1	4.8	0.7	1.5	1.2/2.5	7.7/8.0
2.6464	4.0	4.0	1.1	0.8	1.4/0.7	4.5	0.3	4.7	9.0/9.0	12.6/12.6
*2.6454	4.0	4.0	0.7	0.8	0.7/0.3	4.6	0.1	4.7	5.1/5.1	10.2/10.1

influence on the signal yield in the 2D fit. The uncertainty from this intermediate process is estimated with the same method for the shapes by comparing the yield of the $e^+e^- \rightarrow \Delta^{++}\bar{p}\pi^- + c.c.$ process, which will contribute an uncertainty about 5%. Several possible excited baryons have also been verified and the most likely contribution is found to come from the $N(1710)^+\bar{p} + c.c.$ process with $N(1710)^+ \rightarrow \Delta^{++}\pi^-$. Since the $N(1710)^+\bar{p} + c.c.$ channel is part of the $\Delta^{++}\bar{p}\pi^- + c.c.$ process, the uncertainty is only estimated for the $\Delta^{++}\bar{p}\pi^- + c.c.$ process above 2.6 GeV and the contribution is at most 5.0%. The intermediate states are correlated and result in reduction of the signal yield. A conservative uncertainty is estimated by choosing the largest one among those contributions. All of the systematic uncertainties of the cross section measurement are summarized in Table IV.

VI. CONCLUSION

In this paper, the $e^+e^- \rightarrow \Delta^{++}\bar{\Delta}^{--}$ process is searched for with data taken at c.m. energies from 2.3094 to 2.6464 GeV. There is no significant $e^+e^- \rightarrow \Delta^{++}\bar{\Delta}^{--}$ signal at any energy, while clear signals for the $e^+e^- \rightarrow \Delta^{++}\bar{p}\pi^- + c.c.$ process are observed above 2.6 GeV. Upper limits on the Born cross sections of the $e^+e^- \rightarrow \Delta^{++}\bar{\Delta}^{--}$ process at the 90% CL are extracted; they are comparable to but lower than the predictions in Ref. [12]. With only upper limits, the predicted production ratios among Δ multiplet members in Ref. [9] cannot be addressed. Higher statistics are required for further studies of Δ pair production.

ACKNOWLEDGMENTS

The BESIII collaboration thanks the staff of BEPCII and the IHEP computing center and the supercomputing center of USTC for their strong support. This work is supported in part by National Key R&D Program of China under Contracts No. 2020YFA0406400, No. 2020YFA0406300; National Natural Science Foundation of China (NSFC) under Contracts No. 12105276, No. 11335008, No. 11625523,

No. 11635010, No. 11705192, No. 11735014, No. 11835012, No. 11935015, No. 11935016, No. 11935018, No. 11950410506, No. 11961141012, No. 12022510, No. 12025502, No. 12035009, No. 12035013, No. 12061131003, No. 12122509, No. 12192260, No. 12192261, No. 12192262, No. 12192263, No. 12192264, and No. 12192265; the Chinese Academy of Sciences (CAS) Large-Scale Scientific Facility Program; the CAS Center for Excellence in Particle Physics (CCEPP); Joint Large-Scale Scientific Facility Funds of the NSFC and CAS under Contracts No. U1732263, No. U1832103, No. U1832207, and No. U2032111; CAS Key Research Program of Frontier Sciences under Contracts No. QYZDJ-SSW-SLH003, No. QYZDJ-SSW-SLH040; 100 Talents Program of CAS; The Institute of Nuclear and Particle Physics (INPAC) and Shanghai Key Laboratory for Particle Physics and Cosmology; ERC under Contract No. 758462; European Union’s Horizon 2020 research and innovation programme under Marie Skłodowska-Curie grant agreement under Contract No. 894790; German Research Foundation DFG under Contracts No. 443159800, No. 455635585, Collaborative Research Center CRC 1044, FOR5327, GRK 2149; Istituto Nazionale di Fisica Nucleare, Italy; Ministry of Development of Turkey under Contract No. DPT2006K-120470; National Science and Technology fund; National Science Research and Innovation Fund (NSRF) via the Program Management Unit for Human Resources & Institutional Development, Research and Innovation under Contract No. B16F640076; Olle Engkvist Foundation under Contract No. 200-0605; STFC (United Kingdom); Suranaree University of Technology (SUT), Thailand Science Research and Innovation (TSRI), and National Science Research and Innovation Fund (NSRF) under Contract No. 160355; The Royal Society, UK under Contracts No. DH140054, No. DH160214; The Swedish Research Council; U.S. Department of Energy under Contract No. DE-FG02-05ER41374.

- [1] G. S. Huang and R. B. Ferroli (BESIII Collaboration), *Nat. Sci. Rev.* **8**, nwab187 (2021).
- [2] J. P. Lees *et al.* (BABAR Collaboration), *Phys. Rev. D* **87**, 092005 (2013); **88**, 072009 (2013); M. Ablikim *et al.* (BESIII Collaboration), *Phys. Rev. Lett.* **124**, 042001 (2020).
- [3] M. N. Achasov *et al.* (SND Collaboration), *Phys. Rev. D* **90**, 112007 (2014); V. P. Druzhinin and S. I. Serednyakov, *EPJ Web Conf.* **212**, 07007 (2019); M. Ablikim *et al.* (BESIII Collaboration), *Nat. Phys.* **17**, 1200 (2021).
- [4] M. Ablikim *et al.* (BESIII Collaboration), *Phys. Rev. D* **97**, 032013 (2018); B. Aubert *et al.* (BABAR Collaboration), *Phys. Rev. D* **76**, 092006 (2007).
- [5] M. Ablikim *et al.* (BESIII Collaboration), *Phys. Lett. B* **814**, 136110 (2021).
- [6] M. Ablikim *et al.* (BESIII Collaboration), *Phys. Rev. D* **103**, 012005 (2021); *Phys. Lett. B* **820**, 136557 (2021).
- [7] G. Pakhlova *et al.* (Belle Collaboration), *Phys. Rev. Lett.* **101**, 172001 (2008); M. Ablikim *et al.* (BESIII Collaboration), *Phys. Rev. Lett.* **120**, 132001 (2018).
- [8] V. Pascalutsa, M. Vanderhaeghen, and S. N. Yang, *Phys. Rep.* **437**, 125 (2007).
- [9] M. Karliner, eConf C **010430**, W10 (2001), arXiv:hep-ph/0108106.
- [10] M. Karliner and S. Nussinov, *Phys. Lett. B* **538**, 321 (2002).
- [11] R. L. Workman *et al.* (Particle Data Group), *Prog. Theor. Exp. Phys.* **2022**, 083C01 (2022).
- [12] J. G. Körner and M. Kuroda, *Phys. Rev. D* **16**, 2165 (1977).
- [13] M. Ablikim *et al.* (BESIII Collaboration), *Phys. Rev. D* **99**, 032001 (2019).
- [14] M. Ablikim *et al.* (BESIII Collaboration), *Chin. Phys. C* **41**, 063001 (2017).
- [15] M. Ablikim *et al.* (BESIII Collaboration), *Nucl. Instrum. Methods Phys. Res., Sect. A* **614**, 345 (2010).
- [16] C. H. Yu *et al.*, in *Proceedings of IPAC2016, Busan, Korea* (2016), 10.18429/JACoW-IPAC2016-TUYA01.
- [17] M. Ablikim *et al.* (BESIII Collaboration), *Chin. Phys. C* **44**, 040001 (2020).
- [18] K. X. Huang *et al.*, *Nucl. Sci. Tech.* **33**, 142 (2022).
- [19] S. Agostinelli *et al.* (GEANT4 Collaboration), *Nucl. Instrum. Methods Phys. Res., Sect. A* **506**, 250 (2003).
- [20] Z. Y. Deng *et al.*, *Chin. Phys. C* **30**, 371 (2006).
- [21] R. G. Ping, *Chin. Phys. C* **38**, 083001 (2014).
- [22] M. Ablikim *et al.* (BESIII Collaboration), *Phys. Rev. Lett.* **128**, 062004 (2022).
- [23] G. J. Feldman and R. D. Cousins, *Phys. Rev. D* **57**, 3873 (1998).
- [24] K. Stenson, arXiv:physics/0605236.
- [25] W. L. Yuan, X. C. Ai, X. B. Ji, S. J. Chen, Y. Zhang, L. H. Wu, L. L. Wang, and Y. Yuan, *Chin. Phys. C* **40**, 026201 (2016).
- [26] M. Ablikim *et al.* (BESIII Collaboration), *Phys. Rev. Lett.* **124**, 042001 (2020).
- [27] S. Pacetti, R. Baldini Ferroli, and E. Tomasi-Gustafsson, *Phys. Rep.* **550–551**, 1 (2015).
- [28] Z. Z. Xu, *Introduction to Nuclear and Particle Physics* (Press of University of Science and Technology of China, Hefei, 2009), pp. 250–257; E. Byckling and K. Kajantie, *Particle Kinematics* (John Wiley & Sons Ltd., London, 1971), pp. 58–65.
- [29] R. Wanke, *Data Analysis in High Energy Physics* (Wiley-VCH Verlag GmbH and Co. KGaA, New York, 2013), pp. 263–280.
- [30] B. C. Hunt and D. M. Manley, *Phys. Rev. C* **99**, 055205 (2019).

M. Ablikim,¹ M. N. Achasov,^{12,b} P. Adlarson,⁷² R. Aliberti,³³ A. Amoroso,^{71a,71c} M. R. An,³⁷ Q. An,^{68,55} Y. Bai,⁵⁴ O. Bakina,³⁴ R. Baldini Ferroli,^{27a} I. Balossino,^{28a} Y. Ban,^{44,g} V. Batozskaya,^{1,42} D. Becker,³³ K. Begzsuren,³⁰ N. Berger,³³ M. Bertani,^{27a} D. Bettoni,^{28a} F. Bianchi,^{71a,71c} E. Bianco,^{71a,71c} J. Bloms,⁶⁵ A. Bortone,^{71a,71c} I. Boyko,³⁴ R. A. Briere,⁵ A. Brueggemann,⁶⁵ H. Cai,⁷³ X. Cai,^{1,55} A. Calcaterra,^{27a} G. F. Cao,^{1,60} N. Cao,^{1,60} S. A. Cetin,^{59a} J. F. Chang,^{1,55} W. L. Chang,^{1,60} G. R. Che,⁴¹ G. Chelkov,^{34,a} C. Chen,⁴¹ Chao Chen,⁵² G. Chen,¹ H. S. Chen,^{1,60} M. L. Chen,^{1,55,60} S. J. Chen,⁴⁰ S. M. Chen,⁵⁸ T. Chen,^{1,60} X. R. Chen,^{29,60} X. T. Chen,^{1,60} Y. B. Chen,^{1,55} Y. Q. Chen,³² Z. J. Chen,^{24,h} W. S. Cheng,^{71c} S. K. Choi,⁵² X. Chu,⁴¹ G. Cibinetto,^{28a} S. C. Coen,⁴ F. Cossio,^{71c} J. J. Cui,⁴⁷ H. L. Dai,^{1,55} J. P. Dai,⁷⁶ A. Dbeyssi,¹⁸ R. E. de Boer,⁴ D. Dedovich,³⁴ Z. Y. Deng,¹ A. Denig,³³ I. Denysenko,³⁴ M. Destefanis,^{71a,71c} F. De Mori,^{71a,71c} Y. Ding,³² Y. Ding,³⁸ J. Dong,^{1,55} L. Y. Dong,^{1,60} M. Y. Dong,^{1,55,60} X. Dong,⁷³ S. X. Du,⁷⁸ Z. H. Duan,⁴⁰ P. Egorov,^{34,a} Y. L. Fan,⁷³ J. Fang,^{1,55} S. S. Fang,^{1,60} W. X. Fang,¹ Y. Fang,¹ R. Farinelli,^{28a} L. Fava,^{71b,71c} F. Feldbauer,⁴ G. Felici,^{27a} C. Q. Feng,^{68,55} J. H. Feng,⁵⁶ K. Fischer,⁶⁶ M. Fritsch,⁴ C. Fritsch,⁶⁵ C. D. Fu,¹ Y. W. Fu,¹ H. Gao,⁶⁰ Y. N. Gao,^{44,g} Yang Gao,^{68,55} S. Garbolino,^{71c} I. Garzia,^{28a,28b} P. T. Ge,⁷³ Z. W. Ge,⁴⁰ C. Geng,⁵⁶ E. M. Gersabeck,⁶⁴ A. Gilman,⁶⁶ K. Goetzen,¹³ L. Gong,³⁸ W. X. Gong,^{1,55} W. Gradl,³³ M. Greco,^{71a,71c} M. H. Gu,^{1,55} Y. T. Gu,¹⁵ C. Y. Guan,^{1,60} Z. L. Guan,²¹ A. Q. Guo,^{29,60} L. B. Guo,³⁹ R. P. Guo,⁴⁶ Y. P. Guo,^{11,f} A. Guskov,^{34,a} X. T. H.,^{1,60} W. Y. Han,³⁷ X. Q. Hao,¹⁹ F. A. Harris,⁶² K. K. He,⁵² K. L. He,^{1,60} F. H. Heinsius,⁴ C. H. Heinz,³³ Y. K. Heng,^{1,55,60} C. Herold,⁵⁷ T. Holtmann,⁴ G. Y. Hou,^{1,60} Y. R. Hou,⁶⁰ Z. L. Hou,¹ H. M. Hu,^{1,60} J. F. Hu,^{53,i} T. Hu,^{1,55,60} Y. Hu,¹ G. S. Huang,^{68,55} K. X. Huang,⁵⁶ L. Q. Huang,^{29,60} X. T. Huang,⁴⁷ Y. P. Huang,¹ T. Hussain,⁷⁰ N. Hüskens,^{26,33} W. Imoehl,²⁶ M. Irshad,^{68,55} J. Jackson,²⁶ S. Jaeger,⁴ S. Janchiv,³⁰ E. Jang,⁵² J. H. Jeong,⁵² Q. Ji,¹ Q. P. Ji,¹⁹ X. B. Ji,^{1,60} X. L. Ji,^{1,55} Y. Y. Ji,⁴⁷ Z. K. Jia,^{68,55} P. C. Jiang,^{44,g} S. S. Jiang,³⁷ T. J. Jiang,¹⁶ X. S. Jiang,^{1,55,60} Y. Jiang,⁶⁰ J. B. Jiao,⁴⁷ Z. Jiao,²² S. Jin,⁴⁰ Y. Jin,⁶³ M. Q. Jing,^{1,60} T. Johansson,⁷² X. K.,¹

S. Kabana,³¹ N. Kalantar-Nayestanaki,⁶¹ X. L. Kang,⁹ X. S. Kang,³⁸ R. Kappert,⁶¹ M. Kavatsyuk,⁶¹ B. C. Ke,⁷⁸
A. Khoukaz,⁶⁵ R. Kiuchi,¹ R. Kliemt,¹³ L. Koch,³⁵ O. B. Kolcu,^{59a} B. Kopf,⁴ M. Kuessner,⁴ A. Kupsc,^{42,72} W. Kühn,³⁵
J. J. Lane,⁶⁴ J. S. Lange,³⁵ P. Larin,¹⁸ A. Lavania,²⁵ L. Lavezzi,^{71a,71c} T. T. Lei,^{68,k} Z. H. Lei,^{68,55} H. Leithoff,³³
M. Lellmann,³³ T. Lenz,³³ C. Li,⁴¹ C. Li,⁴⁵ C. H. Li,³⁷ Cheng Li,^{68,55} D. M. Li,⁷⁸ F. Li,^{1,55} G. Li,¹ H. Li,^{68,55} H. B. Li,^{1,60}
H. J. Li,¹⁹ H. N. Li,^{53,i} Hui Li,⁴¹ J. R. Li,⁵⁸ J. S. Li,⁵⁶ J. W. Li,⁴⁷ Ke Li,¹ L. J. Li,^{1,60} L. K. Li,¹ Lei Li,³ M. H. Li,⁴¹ P. R. Li,^{36,j,k}
S. X. Li,¹¹ S. Y. Li,⁵⁸ T. Li,⁴⁷ W. D. Li,^{1,60} W. G. Li,¹ X. H. Li,^{68,55} X. L. Li,⁴⁷ Xiaoyu Li,^{1,60} Y. G. Li,^{44,g} Z. J. Li,⁵⁶ Z. X. Li,¹⁵
Z. Y. Li,⁵⁶ C. Liang,⁴⁰ H. Liang,^{1,60} H. Liang,^{68,55} H. Liang,³² Y. F. Liang,⁵¹ Y. T. Liang,^{29,60} G. R. Liao,¹⁴ L. Z. Liao,⁴⁷
J. Libby,²⁵ A. Limphirat,⁵⁷ D. X. Lin,^{29,60} T. Lin,¹ B. X. Liu,⁷³ B. J. Liu,¹ C. Liu,³² C. X. Liu,¹ D. Liu,^{18,68} F. H. Liu,⁵⁰
Fang Liu,¹ Feng Liu,⁶ G. M. Liu,^{53,i} H. Liu,^{36,j,k} H. B. Liu,¹⁵ H. M. Liu,^{1,60} Huanhuan Liu,¹ Huihui Liu,²⁰ J. B. Liu,^{68,55}
J. L. Liu,⁶⁹ J. Y. Liu,^{1,60} K. Liu,¹ K. Y. Liu,³⁸ Ke Liu,²¹ L. Liu,^{68,55} L. C. Liu,²¹ Lu Liu,⁴¹ M. H. Liu,^{11,f} P. L. Liu,¹ Q. Liu,⁶⁰
S. B. Liu,^{68,55} T. Liu,^{11,f} W. K. Liu,⁴¹ W. M. Liu,^{68,55} X. Liu,^{36,j,k} Y. Liu,^{36,j,k} Y. B. Liu,⁴¹ Z. A. Liu,^{1,55,60} Z. Q. Liu,⁴⁷
X. C. Lou,^{1,55,60} F. X. Lu,⁵⁶ H. J. Lu,²² J. G. Lu,^{1,55} X. L. Lu,¹ Y. Lu,⁷ Y. P. Lu,^{1,55} Z. H. Lu,^{1,60} C. L. Luo,³⁹ M. X. Luo,⁷⁷
T. Luo,^{11,f} X. L. Luo,^{1,55} X. R. Lyu,⁶⁰ Y. F. Lyu,⁴¹ F. C. Ma,³⁸ H. L. Ma,¹ J. L. Ma,^{1,60} L. L. Ma,⁴⁷ M. M. Ma,^{1,60} Q. M. Ma,¹
R. Q. Ma,^{1,60} R. T. Ma,⁶⁰ X. Y. Ma,^{1,55} Y. Ma,^{44,g} F. E. Maas,¹⁸ M. Maggiora,^{71a,71c} S. Maldaner,⁴ S. Malde,⁶⁶ Q. A. Malik,⁷⁰
A. Mangoni,^{27b} Y. J. Mao,^{44,g} Z. P. Mao,¹ S. Marcello,^{71a,71c} Z. X. Meng,⁶³ J. G. Messchendorp,^{13,61} G. Mezzadri,^{28a}
H. Miao,^{1,60} T. J. Min,⁴⁰ R. E. Mitchell,²⁶ X. H. Mo,^{1,55,60} N. Yu. Muchnoi,^{12,b} Y. Nefedov,³⁴ F. Nerling,^{18,d} I. B. Nikolaev,^{12,b}
Z. Ning,^{1,55} S. Nisar,^{10,1} Y. Niu,⁴⁷ S. L. Olsen,⁶⁰ Q. Ouyang,^{1,55,60} S. Pacetti,^{27b,27c} X. Pan,⁵² Y. Pan,⁵⁴ A. Pathak,³²
Y. P. Pei,^{68,55} M. Pelizaesus,⁴ H. P. Peng,^{68,55} K. Peters,^{13,d} J. L. Ping,³⁹ R. G. Ping,^{1,60} S. Plura,³³ S. Pogodin,³⁴ V. Prasad,^{68,55}
F. Z. Qi,¹ H. Qi,^{68,55} H. R. Qi,⁵⁸ M. Qi,⁴⁰ T. Y. Qi,^{11,f} S. Qian,^{1,55} W. B. Qian,⁶⁰ Z. Qian,⁵⁶ C. F. Qiao,⁶⁰ J. J. Qin,⁶⁹
L. Q. Qin,¹⁴ X. P. Qin,^{11,f} X. S. Qin,⁴⁷ Z. H. Qin,^{1,55} J. F. Qiu,¹ S. Q. Qu,⁵⁸ K. H. Rashid,⁷⁰ C. F. Redmer,³³ K. J. Ren,³⁷
A. Rivetti,^{71c} V. Rodin,⁶¹ M. Rolo,^{71c} G. Rong,^{1,60} Ch. Rosner,¹⁸ S. N. Ruan,⁴¹ A. Sarantsev,^{34,c} Y. Schelhaas,³³
K. Schoenning,⁷² M. Scodreggio,^{28a,28b} K. Y. Shan,^{11,f} W. Shan,²³ X. Y. Shan,^{68,55} J. F. Shangguan,⁵² L. G. Shao,^{1,60}
M. Shao,^{68,55} C. P. Shen,^{11,f} H. F. Shen,^{1,60} W. H. Shen,⁶⁰ X. Y. Shen,^{1,60} B. A. Shi,⁶⁰ H. C. Shi,^{68,55} J. Y. Shi,¹ Q. Q. Shi,⁵²
R. S. Shi,^{1,60} X. Shi,^{1,55} J. J. Song,¹⁹ T. Z. Song,⁵⁶ W. M. Song,^{32,1} Y. X. Song,^{44,g} S. Sosio,^{71a,71c} S. Spataro,^{71a,71c} F. Stieler,³³
Y. J. Su,⁶⁰ G. B. Sun,⁷³ G. X. Sun,¹ H. Sun,⁶⁰ H. K. Sun,¹ J. F. Sun,¹⁹ K. Sun,⁵⁸ L. Sun,⁷³ S. S. Sun,^{1,60} T. Sun,^{1,60} W. Y. Sun,³²
Y. Sun,⁹ Y. J. Sun,^{68,55} Y. Z. Sun,¹ Z. T. Sun,⁴⁷ Y. X. Tan,^{68,55} C. J. Tang,⁵¹ G. Y. Tang,¹ J. Tang,⁵⁶ Y. A. Tang,⁷³ L. Y. Tao,⁶⁹
Q. T. Tao,^{24,h} M. Tat,⁶⁶ J. X. Teng,^{68,55} V. Thoren,⁷² W. H. Tian,⁴⁹ W. H. Tian,⁵⁶ Y. Tian,^{29,60} Z. F. Tian,⁷³ I. Uman,^{59b}
B. Wang,¹ B. Wang,^{68,55} B. L. Wang,⁶⁰ C. W. Wang,⁴⁰ D. Y. Wang,^{44,g} F. Wang,⁶⁹ H. J. Wang,^{36,j,k} H. P. Wang,^{1,60}
K. Wang,^{1,55} L. L. Wang,¹ M. Wang,⁴⁷ Meng Wang,^{1,60} S. Wang,^{11,f} T. Wang,^{11,f} T. J. Wang,⁴¹ W. Wang,⁵⁶ W. Wang,⁶⁹
W. H. Wang,⁷³ W. P. Wang,^{68,55} X. Wang,^{44,g} X. F. Wang,^{36,j,k} X. J. Wang,³⁷ X. L. Wang,^{11,f} Y. Wang,⁵⁸ Y. D. Wang,⁴³
Y. F. Wang,^{1,55,60} Y. H. Wang,⁴⁵ Y. N. Wang,⁴³ Y. Q. Wang,¹ Yaqian Wang,^{17,1} Yi Wang,⁵⁸ Z. Wang,^{1,55} Z. L. Wang,⁶⁹
Z. Y. Wang,^{1,60} Ziyi Wang,⁶⁰ D. Wei,⁶⁷ D. H. Wei,¹⁴ F. Weidner,⁶⁵ S. P. Wen,¹ C. W. Wenzel,⁴ D. J. White,⁶⁴ U. Wiedner,⁴
G. Wilkinson,⁶⁶ M. Wolke,⁷² L. Wollenberg,⁴ C. Wu,³⁷ J. F. Wu,^{1,60} L. H. Wu,¹ L. J. Wu,^{1,60} X. Wu,^{11,f} X. H. Wu,³² Y. Wu,⁶⁸
Y. J. Wu,²⁹ Z. Wu,^{1,55} L. Xia,^{68,55} X. M. Xian,³⁷ T. Xiang,^{44,g} D. Xiao,^{36,j,k} G. Y. Xiao,⁴⁰ H. Xiao,^{11,f} S. Y. Xiao,¹
Y. L. Xiao,^{11,f} Z. J. Xiao,³⁹ C. Xie,⁴⁰ X. H. Xie,^{44,g} Y. Xie,⁴⁷ Y. G. Xie,^{1,55} Y. H. Xie,⁶ Z. P. Xie,^{68,55} T. Y. Xing,^{1,60}
C. F. Xu,^{1,60} C. J. Xu,⁵⁶ G. F. Xu,¹ H. Y. Xu,⁶³ Q. J. Xu,¹⁶ X. P. Xu,⁵² Y. C. Xu,⁷⁵ Z. P. Xu,⁴⁰ F. Yan,^{11,f} L. Yan,^{11,f}
W. B. Yan,^{68,55} W. C. Yan,⁷⁸ X. Q. Yan,¹ H. J. Yang,^{48,e} H. L. Yang,³² H. X. Yang,¹ Tao Yang,¹ Y. F. Yang,⁴¹ Y. X. Yang,^{1,60}
Yifan Yang,^{1,60} M. Ye,^{1,55} M. H. Ye,⁸ J. H. Yin,¹ Z. Y. You,⁵⁶ B. X. Yu,^{1,55,60} C. X. Yu,⁴¹ G. Yu,^{1,60} T. Yu,⁶⁹ X. D. Yu,^{44,g}
C. Z. Yuan,^{1,60} L. Yuan,² S. C. Yuan,¹ X. Q. Yuan,¹ Y. Yuan,^{1,60} Z. Y. Yuan,⁵⁶ C. X. Yue,³⁷ A. A. Zafar,⁷⁰ F. R. Zeng,⁴⁷
X. Zeng,^{11,f} Y. Zeng,^{24,h} X. Y. Zhai,³² Y. H. Zhan,⁵⁶ A. Q. Zhang,^{1,60} B. L. Zhang,^{1,60} B. X. Zhang,¹ D. H. Zhang,⁴¹
G. Y. Zhang,¹⁹ H. Zhang,⁶⁸ H. H. Zhang,⁵⁶ H. H. Zhang,³² H. Q. Zhang,^{1,55,60} H. Y. Zhang,^{1,55} J. J. Zhang,⁴⁹ J. L. Zhang,⁷⁴
J. Q. Zhang,³⁹ J. W. Zhang,^{1,55,60} J. X. Zhang,^{36,j,k} J. Y. Zhang,¹ J. Z. Zhang,^{1,60} Jianyu Zhang,^{1,60} Jiawei Zhang,^{1,60}
L. M. Zhang,⁵⁸ L. Q. Zhang,⁵⁶ Lei Zhang,⁴⁰ P. Zhang,¹ Q. Y. Zhang,^{37,78} Shuihan Zhang,^{1,60} Shulei Zhang,^{24,h}
X. D. Zhang,⁴³ X. M. Zhang,¹ X. Y. Zhang,⁴⁷ X. Y. Zhang,⁵² Y. Zhang,⁶⁶ Y. T. Zhang,⁷⁸ Y. H. Zhang,^{1,55} Yan Zhang,^{68,55}
Yao Zhang,¹ Z. H. Zhang,¹ Z. L. Zhang,³² Z. Y. Zhang,⁷³ Z. Y. Zhang,⁴¹ G. Zhao,¹ J. Zhao,³⁷ J. Y. Zhao,^{1,60} J. Z. Zhao,^{1,55}
Lei Zhao,^{68,55} Ling Zhao,¹ M. G. Zhao,⁴¹ S. J. Zhao,⁷⁸ Y. B. Zhao,^{1,55} Y. X. Zhao,^{29,60} Z. G. Zhao,^{68,55} A. Zhemchugov,^{34,a}
B. Zheng,⁶⁹ J. P. Zheng,^{1,55} W. J. Zheng,^{1,60} Y. H. Zheng,⁶⁰ B. Zhong,³⁹ X. Zhong,⁵⁶ H. Zhou,⁴⁷ L. P. Zhou,^{1,60} X. Zhou,⁷³
X. K. Zhou,⁶⁰ X. R. Zhou,^{68,55} X. Y. Zhou,³⁷ Y. Z. Zhou,^{11,f} J. Zhu,⁴¹ K. Zhu,¹ K. J. Zhu,^{1,55,60} L. Zhu,³² L. X. Zhu,⁶⁰
S. H. Zhu,⁶⁷ S. Q. Zhu,⁴⁰ T. J. Zhu,^{11,f} W. J. Zhu,^{11,f} Y. C. Zhu,^{68,55} Z. A. Zhu,^{1,60} J. H. Zou,¹ and J. Zu^{68,55}

(BESIII Collaboration)

- ¹*Institute of High Energy Physics, Beijing 100049, People's Republic of China*
²*Beihang University, Beijing 100191, People's Republic of China*
³*Beijing Institute of Petrochemical Technology, Beijing 102617, People's Republic of China*
⁴*Bochum Ruhr-University, D-44780 Bochum, Germany*
⁵*Carnegie Mellon University, Pittsburgh, Pennsylvania 15213, USA*
⁶*Central China Normal University, Wuhan 430079, People's Republic of China*
⁷*Central South University, Changsha 410083, People's Republic of China*
⁸*China Center of Advanced Science and Technology, Beijing 100190, People's Republic of China*
⁹*China University of Geosciences, Wuhan 430074, People's Republic of China*
¹⁰*COMSATS University Islamabad, Lahore Campus, Defence Road, Off Raiwind Road, 54000 Lahore, Pakistan*
¹¹*Fudan University, Shanghai 200433, People's Republic of China*
¹²*G.I. Budker Institute of Nuclear Physics SB RAS (BINP), Novosibirsk 630090, Russia*
¹³*GSI Helmholtzcentre for Heavy Ion Research GmbH, D-64291 Darmstadt, Germany*
¹⁴*Guangxi Normal University, Guilin 541004, People's Republic of China*
¹⁵*Guangxi University, Nanning 530004, People's Republic of China*
¹⁶*Hangzhou Normal University, Hangzhou 310036, People's Republic of China*
¹⁷*Hebei University, Baoding 071002, People's Republic of China*
¹⁸*Helmholtz Institute Mainz, Staudinger Weg 18, D-55099 Mainz, Germany*
¹⁹*Henan Normal University, Xinxiang 453007, People's Republic of China*
²⁰*Henan University of Science and Technology, Luoyang 471003, People's Republic of China*
²¹*Henan University of Technology, Zhengzhou 450001, People's Republic of China*
²²*Huangshan College, Huangshan 245000, People's Republic of China*
²³*Hunan Normal University, Changsha 410081, People's Republic of China*
²⁴*Hunan University, Changsha 410082, People's Republic of China*
²⁵*Indian Institute of Technology Madras, Chennai 600036, India*
²⁶*Indiana University, Bloomington, Indiana 47405, USA*
^{27a}*INFN Laboratori Nazionali di Frascati, I-00044, Frascati, Italy*
^{27b}*INFN Sezione di Perugia, I-06100, Perugia, Italy*
^{27c}*University of Perugia, I-06100, Perugia, Italy*
^{28a}*INFN Sezione di Ferrara, I-44122, Ferrara, Italy*
^{28b}*University of Ferrara, I-44122, Ferrara, Italy*
²⁹*Institute of Modern Physics, Lanzhou 730000, People's Republic of China*
³⁰*Institute of Physics and Technology, Peace Avenue 54B, Ulaanbaatar 13330, Mongolia*
³¹*Instituto de Alta Investigación, Universidad de Tarapacá, Casilla 7D, Arica, Chile*
³²*Jilin University, Changchun 130012, People's Republic of China*
³³*Johannes Gutenberg University of Mainz, Johann-Joachim-Becher-Weg 45, D-55099 Mainz, Germany*
³⁴*Joint Institute for Nuclear Research, 141980 Dubna, Moscow region, Russia*
³⁵*Justus-Liebig-Universitaet Giessen, II. Physikalisches Institut, Heinrich-Buff-Ring 16, D-35392 Giessen, Germany*
³⁶*Lanzhou University, Lanzhou 730000, People's Republic of China*
³⁷*Liaoning Normal University, Dalian 116029, People's Republic of China*
³⁸*Liaoning University, Shenyang 110036, People's Republic of China*
³⁹*Nanjing Normal University, Nanjing 210023, People's Republic of China*
⁴⁰*Nanjing University, Nanjing 210093, People's Republic of China*
⁴¹*Nankai University, Tianjin 300071, People's Republic of China*
⁴²*National Centre for Nuclear Research, Warsaw 02-093, Poland*
⁴³*North China Electric Power University, Beijing 102206, People's Republic of China*
⁴⁴*Peking University, Beijing 100871, People's Republic of China*
⁴⁵*Qufu Normal University, Qufu 273165, People's Republic of China*
⁴⁶*Shandong Normal University, Jinan 250014, People's Republic of China*
⁴⁷*Shandong University, Jinan 250100, People's Republic of China*
⁴⁸*Shanghai Jiao Tong University, Shanghai 200240, People's Republic of China*
⁴⁹*Shanxi Normal University, Linfen 041004, People's Republic of China*
⁵⁰*Shanxi University, Taiyuan 030006, People's Republic of China*
⁵¹*Sichuan University, Chengdu 610064, People's Republic of China*
⁵²*Soochow University, Suzhou 215006, People's Republic of China*
⁵³*South China Normal University, Guangzhou 510006, People's Republic of China*

- ⁵⁴*Southeast University, Nanjing 211100, People's Republic of China*
⁵⁵*State Key Laboratory of Particle Detection and Electronics, Beijing 100049, Hefei 230026, People's Republic of China*
⁵⁶*Sun Yat-Sen University, Guangzhou 510275, People's Republic of China*
⁵⁷*Suranaree University of Technology, University Avenue 111, Nakhon Ratchasima 30000, Thailand*
⁵⁸*Tsinghua University, Beijing 100084, People's Republic of China*
^{59a}*Turkish Accelerator Center Particle Factory Group, Istinye University, 34010, Istanbul, Turkey*
^{59b}*Near East University, Nicosia, North Cyprus, Mersin 10, Turkey*
⁶⁰*University of Chinese Academy of Sciences, Beijing 100049, People's Republic of China*
⁶¹*University of Groningen, NL-9747 AA Groningen, The Netherlands*
⁶²*University of Hawaii, Honolulu, Hawaii 96822, USA*
⁶³*University of Jinan, Jinan 250022, People's Republic of China*
⁶⁴*University of Manchester, Oxford Road, Manchester M13 9PL, United Kingdom*
⁶⁵*University of Muenster, Wilhelm-Klemm-Strasse 9, 48149 Muenster, Germany*
⁶⁶*University of Oxford, Keble Road, Oxford OX13RH, United Kingdom*
⁶⁷*University of Science and Technology Liaoning, Anshan 114051, People's Republic of China*
⁶⁸*University of Science and Technology of China, Hefei 230026, People's Republic of China*
⁶⁹*University of South China, Hengyang 421001, People's Republic of China*
⁷⁰*University of the Punjab, Lahore-54590, Pakistan*
^{71a}*University of Turin, I-10125, Turin, Italy*
^{71b}*University of Eastern Piedmont, I-15121, Alessandria, Italy*
^{71c}*INFN, I-10125, Turin, Italy*
⁷²*Uppsala University, Box 516, SE-75120 Uppsala, Sweden*
⁷³*Wuhan University, Wuhan 430072, People's Republic of China*
⁷⁴*Xinyang Normal University, Xinyang 464000, People's Republic of China*
⁷⁵*Yantai University, Yantai 264005, People's Republic of China*
⁷⁶*Yunnan University, Kunming 650500, People's Republic of China*
⁷⁷*Zhejiang University, Hangzhou 310027, People's Republic of China*
⁷⁸*Zhengzhou University, Zhengzhou 450001, People's Republic of China*

^aAlso at the Moscow Institute of Physics and Technology, Moscow 141700, Russia.

^bAlso at the Novosibirsk State University, Novosibirsk, 630090, Russia.

^cAlso at the NRC "Kurchatov Institute," PNPI, 188300, Gatchina, Russia.

^dAlso at Goethe University Frankfurt, 60323 Frankfurt am Main, Germany.

^eAlso at Key Laboratory for Particle Physics, Astrophysics and Cosmology, Ministry of Education; Shanghai Key Laboratory for Particle Physics and Cosmology; and Institute of Nuclear and Particle Physics, Shanghai 200240, People's Republic of China.

^fAlso at Key Laboratory of Nuclear Physics and Ion-beam Application (MOE) and Institute of Modern Physics, Fudan University, Shanghai 200443, People's Republic of China.

^gAlso at State Key Laboratory of Nuclear Physics and Technology, Peking University, Beijing 100871, People's Republic of China.

^hAlso at School of Physics and Electronics, Hunan University, Changsha 410082, China.

ⁱAlso at Guangdong Provincial Key Laboratory of Nuclear Science, Institute of Quantum Matter, South China Normal University, Guangzhou 510006, China.

^jAlso at Frontiers Science Center for Rare Isotopes, Lanzhou University, Lanzhou 730000, People's Republic of China.

^kAlso at Lanzhou Center for Theoretical Physics, Lanzhou University, Lanzhou 730000, People's Republic of China.

^lAlso at the Department of Mathematical Sciences, IBA, Karachi, Pakistan.